

# Effect of Fe doping on the terahertz conductivity of GaN single crystals

Filip Kadlec<sup>1</sup>, Christelle Kadlec<sup>1</sup>, Tanya Paskova<sup>2</sup> and Keith Evans<sup>2</sup>

<sup>1</sup> Institute of Physics, Academy of Sciences of the Czech Republic, Na Slovance 2, 182 21 Prague 8, Czech Republic

<sup>2</sup> Kyma Technologies, Inc., Raleigh, NC 27617, USA

Received 10 December 2009, in final form 14 January 2010

Published 23 March 2010

Online at [stacks.iop.org/JPhysD/43/145401](http://stacks.iop.org/JPhysD/43/145401)

## Abstract

Bulk single crystals of GaN with different degrees of Fe doping were studied using time-domain terahertz spectroscopy at high temperatures. Features due to free carriers were observed in the complex permittivity spectra with a pronounced dependence on both doping and temperature. Fitting the spectra using the Drude model made it possible to deduce a defect ionization energy of 16 meV in the undoped sample while the spectra of doped samples are consistent with an ionization energy of 60 meV. Also, the free carrier concentrations at temperatures from 300 to 900 K were estimated.

(Some figures in this article are in colour only in the electronic version)

## 1. Introduction

Gallium nitride is a technologically important material with a wide range of both present and prospective applications. Since the success in epitaxial growth of GaN thin films (see [1] for a review), it has been largely employed in light-emitting diodes, LED displays, and lasers. In the past few years, there has been a rapid development in technologies aiming at the production of bulk GaN; its future uses include, e.g., high-power high-frequency operating field effect transistors, radars and power amplifiers [2]. The epitaxial growth often uses sapphire substrates, and the technology leads to an unintentional n-doping of GaN; O and Si are the main residual impurities at the origin of dc conductivity [3]. For compensation of these donors, doping by Fe can be used; Fe acceptors substitute for Ga and substantially increase the resistivity [4]. In order to achieve optimal properties of the doped crystals, a deeper knowledge of the underlying physical properties of bulk GaN, namely their conductivity mechanisms, is required. From the point of view of high-power applications which may lead to self-heating [5], the properties at higher temperatures are of particular importance. However, standard transport measurements are challenging owing to difficulties in producing low resistivity contacts to the highly resistive GaN material.

Terahertz (THz) spectroscopy is an alternative technique and a convenient tool for studying the dynamical conductivity of GaN. It was shown that the free carriers follow the Drude

model [6] with a plasma frequency in the THz range. Small deviations from the Drude model were reported and studied [7], and the THz spectra were shown to depend on the carrier concentration [8]. In this paper, we study experimentally the THz response of bulk GaN crystals with varying Fe doping and at variable temperatures.

## 2. Sample preparation

The samples were grown in a vertical hydride vapour phase epitaxy hot-wall reactor at a sub-atmospheric pressure. The single crystals were deposited at a rate of  $150 \mu\text{m h}^{-1}$  on *c*-plane (0001) sapphire substrates with an AlN template layer, in the downstream part of the reactor where GaCl and NH<sub>3</sub> transported by the N<sub>2</sub> gas react. The substrates were maintained at a temperature of  $T \approx 1000^\circ\text{C}$ . As an Fe source for doping, a variable flow of bis(cyclopentadienyl)iron was introduced into the reactor via N<sub>2</sub> carrier gas. Once the substrates were removed, the GaN crystals were cut and polished to the shape of slabs with optical quality surfaces and thicknesses ranging from 0.5 to 1.2 mm. Four different samples were measured: one undoped, no 1 (AH939), and three doped, nos 2–4 (AE492, AE535 and AE782; these fabrication labels were used also in [9, 10]). Their Fe atom concentrations were determined by means of secondary ion mass spectrometry as  $3 \times 10^{17} \text{ cm}^{-3}$ ,  $7 \times 10^{17} \text{ cm}^{-3}$  and  $3 \times 10^{18} \text{ cm}^{-3}$ , respectively.

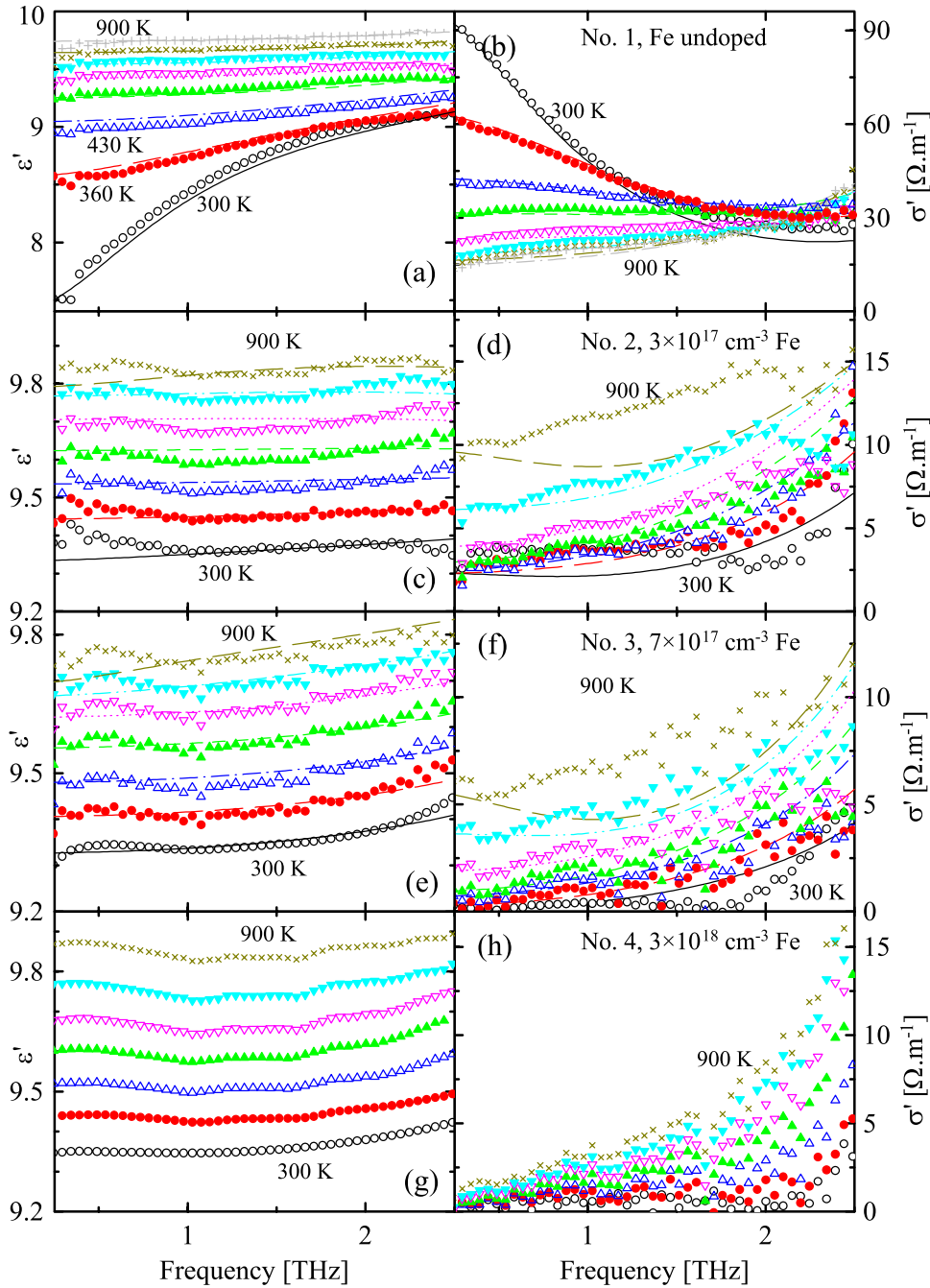


**Figure 1.** Real permittivity (left panels) and conductivity (right panels) spectra of the samples. Points represent experimental data and lines show fits by using equation (1).

### 3. Experimental details

Our custom-made experimental setup for time-domain THz spectroscopy was based on a Ti:sapphire laser oscillator providing 810 nm, 80 fs pulses at a 76 MHz repetition rate. The pulses excited an interdigitated photoconducting emitter [11] which generated linearly polarized THz pulses. A weak part of the laser beam was directed on a 1 mm thick (110) cut ZnTe crystal for electro-optic sampling of the transmitted THz waves. The whole THz beam was enclosed in a vacuum chamber (about 20 mbar) in order to avoid water vapour absorption. The samples were placed in a furnace with optical

ports, using a clear aperture of 3 to 7 mm, and heated up to  $T = 900$  K in steps of 100 K, except for sample no 1 where the temperature of 400 K was replaced by 360 and 430 K. The instrument covered a frequency range 0.25–2.5 THz.

### 4. Results and evaluation

From the complex transmittance, we numerically calculated the spectra of complex refractive index  $\hat{N}(\nu)$  which we converted to permittivity  $\hat{\epsilon}(\nu) \equiv \epsilon' + i\epsilon'' = \hat{N}^2(\nu)$  and conductivity spectra,  $\hat{\sigma}(\nu) = -2\pi\nu\epsilon_0\hat{\epsilon}(\nu)$ ;  $\epsilon_0$  denotes the vacuum permittivity. Symbols in figure 1 show the real parts,

$\varepsilon'(\nu)$  and  $\sigma'(\nu)$ . Signatures of free carrier transport can be clearly seen—even a relatively weak conductivity shows up as a non-vanishing  $\sigma'$  in the low-frequency part. This feature is the strongest for the undoped sample where it clearly gives rise to a Drude peak and it decreases upon Fe doping. For the highest doped sample (no 4), no signs of free charge carriers are visible at any temperature.

As a common trend, the  $\varepsilon'(\nu)$  spectra display a monotonic increase upon heating. For all Fe doped samples, they are almost flat, except for small experimental artefacts and/or noise. In the upper frequency parts of the spectra of samples (no 3, 4) with higher doping (figures 1(e) and (g)), an increase with frequency is seen, similar to previous observations [8]. We attribute this to a contribution of a broad phonon absorption beyond our accessible frequency range.

This term also influences the  $\sigma'(\nu)$  (i.e.  $\varepsilon''(\nu)$ ) spectra in their high-frequency part. From the fitting described below it clearly appears that without such a term, the conductivity increase above  $\nu > 1$  THz would not be observed.

The most interesting information, however, is related to the low-frequency parts of  $\sigma'(\nu)$ ; it is that about free charge carriers. The temperature dependence of these low-frequency parts is strongly influenced by doping. While it decreases with  $T$  in sample no 1 (figure 1(b)), an increase upon heating is observed in the lower Fe doped samples no 2 and no 3 (figures 1(d) and (f)); in the latter case, heating is necessary to bring up the Drude-like contribution. Finally, for sample no. 4, the free carrier conductivity is not visible at any temperature (figure 1(h)).

We fitted the  $\hat{\varepsilon}(\nu)$  spectra of the samples displaying signs of electrical conduction. In view of the observed features, we found the same model as used in [8] to be the best suited ( $\omega = 2\pi\nu$ ):

$$\hat{\varepsilon}(\omega) = \frac{\omega_p^2}{\omega^2 - i\omega\gamma} + \frac{f_0}{\omega_0^2 - \omega^2 - i\omega\Gamma} + \varepsilon_\infty \quad (1)$$

with the plasma frequency given by  $\omega_p^2 = Ne_0^2/m_0m^*\varepsilon_0$ . Here,  $e_0$  and  $m_0$  denote the free electron charge and mass, respectively. Equation (1) contains two frequency-dependent terms: (i) a Drude-like plasma of free charge carriers with a concentration  $N$ , effective mass  $m^*$  and a mean collision rate  $\gamma$  and (ii) an overdamped harmonic oscillator with oscillator strength  $f_0$ , eigenfrequency  $\omega_0$  and damping  $\Gamma$ , describing the broad features at higher frequencies. The constant  $\varepsilon_\infty$  accounts for contributions of all modes far beyond the THz region.

First, the complex room-temperature spectrum of the undoped sample (no 1) alone was fitted; the result is shown by solid lines in figures 1(a) and (b). The extrapolated value of static conductivity is  $\sigma_{dc} \approx 1 \Omega^{-1} \text{cm}^{-1}$ . Owing to the pronounced slope in the real part, it is possible to reliably determine the angular plasma frequency  $\omega_p = 8.3 \times 10^{12} \text{ rad s}^{-1}$  and the scattering time  $\tau \equiv 1/\gamma = 160 \text{ fs}$ . Assuming that the free charge carriers are electrons with an effective mass [12] of  $m^* = 0.2$ , one can calculate their concentration,  $N(300 \text{ K}) = 4 \times 10^{15} \text{ cm}^3$  and mobility  $\mu = 1440 \text{ cm}^2 \text{ V}^{-1} \text{ s}^{-1}$ . These results are in agreement with the values determined by THz spectroscopy and reported earlier for undoped GaN [6].

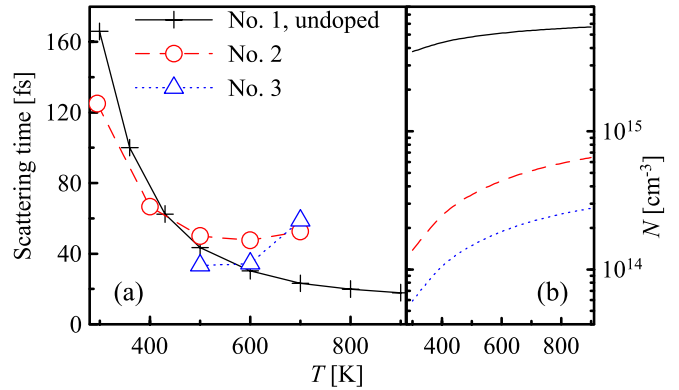


**Figure 2.** Free carrier scattering times  $\tau$  (a) and concentrations (b) estimated from spectra fitting as a function of  $T$ .

Further, we performed a common fit of the spectra at all temperatures. We assumed a linear temperature dependence of  $\varepsilon_\infty$  and the oscillator transverse frequency was fixed at  $\omega_0/2\pi = 5$  THz; its strength was assumed to be constant in  $T$  and its damping  $\Gamma$  linearly proportional to  $T$ . Thus, it was possible to describe the high-frequency part of the spectra. In the weak-doping approximation, the concentration of free electrons can be written as  $N(T) = N_0 \exp(-E_D/k_B T)$  where  $E_D$  is the defect ionization energy and  $k_B$  the Boltzmann constant. The collision rate  $\gamma$  was allowed to vary with  $T$  without limitations. The solid lines in figures 1(a) and (b) show the fit matching well with the experimental data; the best match is found for a value of  $E_D = 16 \pm 3$  meV. The solid lines in figure 2 show the obtained functions  $\tau(T)$  and  $N(T)$ .

The spectra of sample no 2 with low Fe doping display much smaller spectral features than those of the undoped sample (no 1). Thus, it was necessary to fit them together; we used the same model (equation (1)) and temperature dependence of parameters. We found the room-temperature concentration of electrons to be  $N(300 \text{ K}) = 1.4 \times 10^{14} \text{ cm}^3$ , while the defect ionization energy was substantially higher,  $E_D = 60 \pm 10$  meV. This leads to a steeper increase in  $N$  upon heating (figure 2(b)). The model does not agree very well with the experimental data at the highest temperatures ( $T > 700$  K), which is probably a sign of a supplementary absorption mechanism in this temperature range. Therefore, the values of the scattering time  $\tau$  become unreliable and they are not shown in figure 2(a). Nevertheless, since the model describes well the conductivity spectra in the lowest part of the THz range, it should still provide a useful estimate of the free carrier concentration up to the highest temperatures.

In sample no 3, the even higher level of doping suppresses the features linked to the free carrier absorption at room temperature (figures 1(e) and (f)). However, upon heating above 500 K,  $\sigma'$  increases at lower frequencies. Due to its low values, the fit performed for this sample does not provide unambiguously the concentration of the free electrons. Therefore, we assumed a concentration inversely proportional to the Fe doping level, i.e.  $N(300 \text{ K}) = 6 \times 10^{13} \text{ cm}^3$ . In this way, with the same value of  $E_D = 60$  meV, a good agreement with the measured spectra was achieved. Analogously to sample no 2, the validity of the model at

the highest temperatures is limited; thus, values of  $\tau$  can be estimated only in the range  $500 \text{ K} \leq T \leq 700 \text{ K}$ .

Finally, no features related to electrical conductivity are observed in the spectra of sample no 4 with the highest doping. By comparing the spectra at the highest temperatures with those of sample no 3, and assuming the same values of  $\gamma$ , we can estimate that the carrier concentration decreased by a factor of four or more.

## 5. Discussion

In the undoped sample, the activation energy of 16 meV is very close to that determined from transport measurements in intentionally Si-doped samples [13]. By contrast, the THz mobility is one order of magnitude higher, while the room-temperature concentration of carriers in THz experiments is about two orders of magnitude lower. This means that the interactions of carriers dominantly contributing to the THz conductivity, where local motion across about tens of nanometres is sensed, are different from those occurring in the long-range transport; we attribute this fact to short-scale spatial doping inhomogeneities. The energy level of 16 meV apparently corresponds to the residual donor—either O or Si—as reported earlier based on Hall-mobility measurements on electron-irradiated samples [14]. The activation energy of 60 meV in doped samples (nos 2 and 3) is clearly linked to the Fe doping; in agreement with previous works [14, 15] we attribute it to the N vacancy donor  $V_N$ . The concentration of these donors appears to increase at low levels of Fe doping; this might be because the doping leads to a decrease in the Fermi level whereby the vacancies would become energetically more stable. In this way, Fe atoms could stabilize the N vacancies, or even Fe– $V_N$  complexes might form. Since figure 3 of [4] displays only a partial agreement between experimental and simulated EXAFS spectra, a part of the Fe dopants probably occupy other crystal sites. Therefore, our hypotheses are not in contradiction to the observation of  $\text{Fe}_{\text{Ga}}$  reported in [4].

For the undoped sample (no 1),  $\tau(T)$  data obtained from fits (figure 2) show a monotonic decrease, apparently linked to the electron–phonon scattering increasing on heating. For the low doped sample (no 2), the same trend is observed at lower temperatures, however, around 600 K,  $\tau$  levels off. Upon further heating above 700 K, the model described by equation (1) departs from our experimental data, therefore  $\tau$  cannot be reliably determined. This holds also for the higher doped sample (no 4); values of  $\tau$  similar to those in samples no 1 and no 2 are observed at medium temperatures. For sample no 3 at low temperatures,  $\tau$  cannot be determined owing to the absence of the Drude contribution. The deviation of our model from the data at the highest temperatures suggests that the energy scheme may be more complex than that we take into account; however, the current knowledge of the energy levels in Fe:GaN does not enable us to set up a more appropriate model.

We also note that, as  $\sigma'(\nu)$  according to the Drude model increases steeply towards low frequencies, measurements at microwave frequencies might provide even more sensitivity for doped samples.

## 6. Conclusion

In conclusion, we have studied the impact of Fe doping on the THz spectra of GaN crystals in view of their future use above room temperature. While doping leads to a suppression of conductivity at room temperature, heating the crystals has the opposite effect. From the temperature dependences of the spectra, we have determined defect ionization energies consistent with those observed earlier and temperature dependences of the free carrier concentrations. Our results are expected to contribute to both the fundamental understanding of carrier transport and the technological use of GaN crystals.

## Acknowledgments

The support by the Czech Academy of Sciences (project AVOZ 10100520) as well as by MDA under the HQ0147-09-C-0005 contract for bulk GaN characterization is acknowledged. The authors would like to thank Dr David Look for useful discussions.

## References

- [1] Pearton S J, Abernathy C R and Fan Ren 2006 *Gallium Nitride Processing for Electronics, Sensors and Spintronics* (Berlin: Springer)
- [2] Keller S, Wu Y-F, Parish G, Ziang N, Xu J J, Keller B P, DenBaars S P and Mishra U K 2001 Gallium nitride based high power heterojunction field effect transistors: process development and present status at ucsb *IEEE Trans. Electron Devices* **48** 552–8
- [3] Moore W J, Freitas J A Jr, Braga G C B, Molnar R J, Lee S K, Lee K Y and Song I J 2001 Identification of Si and O donors in hydride-vapor-phase epitaxial GaN *Appl. Phys. Lett.* **79** 2570–2
- [4] Kumagai Y, Satoh F, Togashi R, Murakami H, Takemoto K, Iihara J, Yamaguchi K and Koukitu A 2006 Fe-doped semi-insulating GaN substrates prepared by hydride vapor-phase epitaxy using GaAs starting substrates *J. Cryst. Growth* **296** 11–14
- [5] Asif Khan M *et al* 2000 GaN–AlGaN heterostructure field-effect transistors over bulk GaN substrates *Appl. Phys. Lett.* **76** 3807–9
- [6] Zhang W, Azad A K and Grischkowsky D 2003 Terahertz studies of carrier dynamics and dielectric response of n-type, freestanding epitaxial GaN *Appl. Phys. Lett.* **82** 2841–3
- [7] Tsai T-R, Chen S-J, Chang C-F, Hsu S-H, Lin T-Y and Chi C-C 2006 Terahertz response of GaN thin films *Opt. Express* **14** 4898–907
- [8] Guo H C, Zhang X H, Liu W, Yong A M and Tang S H 2009 Terahertz carrier dynamics and dielectric properties of GaN epilayers with different carrier concentrations *J. Appl. Phys.* **106** 063104
- [9] Fang Z-Q, Clafflin B, Look D C, Elhamri S, Smith H E, Mitchel W C, Hanser D, Preble E A and Evans K R 2008 Deep centers in semi-insulating Fe-doped native GaN substrates grown by hydride vapour phase epitaxy *Phys. Status Solidi c* **5** 1508–11
- [10] Freitas J A Jr, Gowda M, Tischler J G, Kim J-H, Liu L and Hanser D 2008 Semi-insulating gan substrates for high-frequency device fabrication *J. Cryst. Growth* **310** 3968–72

- [11] Dreyhaupt A, Winnerl S, Dekorsy T and Helm M 2005 High-intensity terahertz radiation from a microstructured large-area photoconductor *Appl. Phys. Lett.* **86** 121114
- [12] Vurgaftman I and Meyer J R 2003 Band parameters for nitrogen-containing semiconductors *J. Appl. Phys.* **94** 3675–96
- [13] Ng H M, Doppalapudi D, Moustakas T D, Weimann N G and Eastman L F 1998 The role of dislocation scattering in n-type GaN films *Appl. Phys. Lett.* **73** 821–3
- [14] Look D C, Reynolds D C, Hemsley J W, Sizelove J R, Jones R L and Molnar R J 1997 Defect donor and acceptor in GaN *Phys. Rev. Lett.* **79** 2273–6
- [15] Look D C, Farlow G C, Drevinsky P J, Bliss D F and Sizelove J R 2003 On the nitrogen vacancy in GaN *Appl. Phys. Lett.* **83** 3525–7